Fan, G.D.; Zheng, M.Y.; Hu, X.S.; Wu, K.; Gan, W.M.; Brokmeier, H.G.:

Internal friction and microplastic deformation behavior of pure magnesium processed by equal channel angular pressing

In: Materials Science and Engineering A (2012) Elsevier

DOI: 10.1016/j.msea.2012.10.083

Internal friction and microplastic deformation behavior of pure magnesium processed by equal channel angular pressing

G.D. Fan[a], M.Y. Zheng[a,*], X.S. Hu[a], K. Wu[a], W.M. Gan[b], H.G. Brokmeier[b,c]

[a] School of Materials Science and Engineering, Harbin Institute of Technology, Harbin 150001, P. R. China

[b] Institute of Materials Research, Helmholtz-Zentrum-Geesthacht (HZG), Outstation at FRM-II, Garching D-85748, Germany

[c] Institute of Materials Science and Engineering, Clausthal University of Technology, Clausthal-Zellerfeld D-38678, Germany

* zhenghe@hit.edu.cn, Tel: 86-451-86402291, Fax: 86-451-86413922

Abstract

Equal channel angular pressing (ECAP) was performed on the as-extruded commercial pure magnesium at 250 °C for 4 passes. The internal friction of the ECAPed pure Mg as a function of strain amplitude was investigated by dynamic mechanical analyzer (DMA), and the cyclic microplasticity of pure Mg was investigated by tensile loading and unloading test. After ECAP processing, the grain size is significantly refined, the texture component with basal planes parallel to extrusion direction is replaced by a new stronger one with basal planes having a tilting angle of about 40º to the extrusion direction. The stress in microplastic region is reduced with increasing ECAP passes, while the internal friction increases. The internal friction of Mg at high strain amplitude is closely related to microplastic deformation and can be interpreted by dislocation mechanism. The Granato and Lücke model only satisfies in anelastic regions, while the internal friction in microplastic deformation region should be explained in terms of the internal friction model postulated by Peguin. The internal friction related to microplasticity can be divided into two parts with different activation volumes of dislocation motion, which correspond to the two regions of microplasctic deformation process. The initial stage associated with dislocation motion on basal plane shows larger activation

volume and lower friction stress of dislocations. The second stage related to the annihilation and tangle of dislocations is characterized by larger hardening exponent and friction stress.

Keywords: Magnesium; ECAP; Cyclic loading; Internal friction; Microplasticity; Texture

1. Introduction

The macroplastic deformation mechanisms of most materials are well studied, while their plasticity occurring below the macroyield point (microplastic deformation) is understood poorly. In fact, the structural components always undergo repeated microplastic deformation when they are in service. The microplasticity determines various properties of the metals, such as fatigue strength [1, 2], dimensional stability [3], and various relaxation phenomena, such as damping (internal friction) behavior [4]. It is a very useful method to study the microplasticity of materials by the analysis of strain amplitude dependent internal friction [5, 6], which makes it possible to quantify the onset strain of microplasticity, the dynamics of changes of the microstructure in the materials or also determine, for example, the size of the activation volume of dislocation motion of microplastic deformation process. However, the processes of microplastic deformation and internal friction were always studied theoretically and experimentally in separate investigations. The strain dependent internal friction is explained as the result of reversible movement of the dislocations around the initial positions which do not change during measurements, i.e., it is an anelastic process. While microplastic deformation process is associated with the breakaway from strong pinning points, subsequent motion and interaction of the dislocations. Few works [5, 6] have been performed on the research of microplasticity by the analysis of strain amplitude effect on internal friction, which is usually divided into three regions, namely the regions in which the internal friction is

strain independent, weakly dependent and strongly dependent. The last part is closely related to microplasticity [4, 5].

Mg and its alloys are characterized by low density and high damping capacity. Equal channel angular pressing (ECAP) offers great potential to modify the microstructures of Mg alloys, thus improve their mechanical property [7, 8] and damping capacity [9, 10]. In the present research, pure magnesium was selected as the experimental material to minimize the influences of secondary phases and solute atoms on microplasticity. ECAP was used to modify the microstructure of the pure Mg, such as the grain size and texture. The present research tries to relate the internal friction with usual tensile property in the microplastic range, in order to shed light on the mechanism of microplastic deformation and internal friction of pure Mg.

2. Experimental techniques

A cast commercial pure Mg (99.90 wt.%) was extruded at 350 °C to a rectangular bar with a reduction ratio of 12:1. The 10 × 10 × 60 mm^3 rectangular billets were machined from the extrusion bars for ECAP. The outer and interior angles of ECAP die were $\psi = 37^o$ and $\Phi = 90^o$, respectively. The ECAP was conducted at 250 ^oC for 4 passes using route B_C, in which the specimen is rotated by $\Phi = 90^o$ in the same direction between each pass. The microstructures of the pure Mg were examined with Olympus DP11 optical microscope (OM). Neutron diffractometer at TEX-2 (GKSS Research Center, Germany) was used to measure the texture. A bulk sample with gauge dimensions of 10 × 10 × 10 mm^3 was cut from the center part of pure Mg for texture measurement.

Tensile tests were performed at room temperature using an Instron 5569 universal test

machine at a crosshead speed of 10 MPa/min. The dogbone-shaped specimens with gauge dimensions of 6 × 2 × 10 mm^3 were used for tensile tests. Microstrain tensile tests were also carried out in dynamic mechanical analyzer (DMA) TA Q800 using tensile mode at a crosshead speed of 8 MPa/min with a strain sensitivity of 1×10^{-6}. The specimen dimension for microstrain tensile tests is 15 × 2 × 1 mm^3. The tensile axes of all the tensile specimens were parallel to the extrusion direction of the as-extruded and as-ECAPed billets.

The internal friction tests were carried out by DMA with single cantilever vibration mode. The specimen dimension for internal friction measurements is 35 × 10 × 1 mm^3. Measurements of internal friction at ambient temperature were made at various strain amplitude range from 4×10^{-6} to 1.8×10^{-3} with vibration frequency of 1 Hz.

3. Results and discussion

3.1. Microstructure

Fig. 1 shows the typical optical microstructures of pure Mg after extrusion and EX－ECAP with 1－4 passes. The average grain size of the as-extruded pure Mg is about 71 μm. The well-defined grain boundaries and equiaxed grains indicate that dynamic recrystallization (DRX) takes place during the extrusion. After being processed by ECAP at 250 ^oC for 1 pass, the grain size is significantly refined to about 23 μm. After ECAP processing for 2 passes, the average grain size is further refined to about 15 μm. There are still some elongated coarse grains surrounded by smaller equiaxed grains in some regions. After being processed by ECAP for 4 passes, the pure Mg exhibits more homogeneous microstructure with average grain size of about 6 μm, as shown in Fig. 1(d).

3.2. Texture evolution

The (0002) and $(10\bar{1}0)$ pole figures of pure Mg processed by extrusion and subsequent ECAP are shown in Fig. 2. The as-extruded Mg exhibits a texture with most of the basal planes nearly parallel to the extrusion direction (ED). After 1 pass ECAP processing, a new stronger texture component with basal planes having a tilting angle of about 35º to ED appears, which can be attributed to the more activations of the pyramidal Ⅱ <*c* + *a*> sliding [11]. But the stronger component with basal planes parallel to the ED still remains. The basal pole distribution becomes more unsymmetrical with increasing ECAP passes and forms a maximum component locating at about 40º from ND (normal direction) towards ED and 20º from ND towards TD. And the texture component with basal planes parallel to ED becomes much weaker. The gradual increase of the Schmid factor for basal slip with increasing ECAP passes may have an important influence on the microplasticity and internal friction of Mg.

3.3. Cyclic microplasticity

Fig. 3 shows the tensile stress－strain curves of the extruded and ECAPed pure Mg in microstrain range. It is observed that the tensile curves depart from straight lines around the strain of 1×10^{-4}. With increasing ECAP passes, the tensile stress at a given strain is reduced gradually. Fig. 4 displays the loading–unloading hysteresis loops of pure Mg measured by DMA using tensile mode with the maximal loading force of 18N. As shown in Fig. 5, the cyclic tension curves in larger strain range were also measured by tensile testing machine, the strain sensitivity of which is not high enough at the beginning of microplastic deformation. So the plastic deformation behavior of pure Mg in the whole microstrain region is obtained by combining the results of both Fig. 4 and 5. Fig. 6 shows the schematic curve of cyclic loading hysteresis loops and relevant parameters on the loading–unloading hysteresis loops.

It can be seen in Fig. 4 that the initial segment of the deformation diagram of pure Mg is linear below the strain of about 1×10^{-4}. When the specimens are unloaded with higher strain and then reloaded, the flow curve exhibits a closed loop whose width increases with the amount of plastic strain. It also can be seen that the as-extruded pure Mg shows higher cyclic tensile stress than that of as-ECAPed specimens.

As shown in Fig. 6, at the peak stress, the applied stress σ_p is the sum of the friction stress σ_f and the back stress σ_b [12, 13]

$$\sigma_p - \sigma_b = \sigma_f \tag{1}$$

The friction stress σ_f corresponds to the resistance the dislocations have to overcome to keep moving in the lattice. The back stress σ_b is associated with piled-up dislocations that are created after overcoming the friction stress.

As the external load is removed and the dislocations begin to move under the effect of back stresses under the condition

$$\sigma_b - \sigma_y = \sigma_f \tag{2}$$

σ_y is the yield stress upon unloading. Consequently, the reverse plastic flow in the unloading of a preloaded specimen will begin when the external stress changes by the quantity $\sigma_p - \sigma_y = 2\sigma_f$. Fig. 7 shows the development of friction stress, which slightly decreases below the strain of about 1×10^{-3}, then increasing rapidly afterward.

Fig. 8 shows the relationship between the tensile stress and plastic strain of pure Mg. In the coordinates $\log \sigma$ – $\log \varepsilon_p$, the experimental points fit straight lines so that the experimentally obtained points can be expressed by the equation

$$\sigma = B\varepsilon_p{}^n \tag{3}$$

The factors B and n are material- and experiment-sensitive constants, the values of n are shown in Table 1. Thus the microplastic deformation process of pure Mg can be divided into three regions. The microplastic region I corresponds to the plastic strain below 2×10^{-4} (Fig. 8a and b), the amount of hardening exponents of pure Mg are about 0.40. When the plastic strain is higher than 2×10^{-4} but lower than another critical value of 1×10^{-3} (Fig. 8b), the deformation process enters into microplastic region Ⅱ with an increase of the slopes of straight lines to 0.6. With a further increase of plastic strain the hardening exponents show a marked decrease (Fig. 8b), which is the manifestation that the transition from micro- to macroplastic deformation takes place.

The anelastic strains as a function of strain of pure Mg are presented in Fig. 9. The anelastic strain shows a rapid increase after an applied strain of about 1×10^{-4}, and saturates after a strain of 0.01–0.02, then decreases at larger strains (Fig. 9b). The ECAPed pure Mg shows larger anelastic strain than the extruded one. And with increasing the ECAP passes, the anelastic strain increases gradually.

Fig. 10 shows the development of normalized secant elastic modulus (E_s, defined in Fig. 6) of pure Mg as a function of true strain. The experimental values were normalized to the initial (elastic) slope of the stress–strain curve for each specimen such that the normalized E_s =1 corresponds to the nominal value for pure Mg, E = 42 GPa. The overall behavior is generally similar for all materials. The values of secant elastic modulus tend to be the value of elastic modulus E as the strain approaches zero. The secant elastic modulus significantly decreases when true strain is higher than 1×10^{-4}, and reaches a minimum at the strain of about 0.01, then slightly increases afterwards. With increasing the number of ECAP passes, the secant

elastic modulus is gradually reduced, and it is decreased by up to 50% for 4 pass ECAP processed pure Mg.

3.4. The relationship between internal friction (IF) and microplasticity

The strain amplitude dependent IF curves of pure Mg at room temperature are presented in Fig. 11. The IF is made up of a strain amplitude independent component and a strain amplitude dependent component. The two components are separated at a critical strain amplitude ε_{cr1}. The IF values of the pure Mg increase after ECAP processing, and ECAP-4P pure Mg shows the highest IF value. The IF mechanism of cast and wrought Mg alloys [14-16] is usually interpreted in terms of dislocation theory developed by Granato and Lücke [17] (G-L). However, in fact, G-L model was mainly developed for fcc metals with weak interaction between dislocation line and pinning points at relatively low temperatures. In the present case, though the interaction between dislocation line on basal sliding plane and impurity atoms is relatively weak in commercial pure Mg, the G-L model's applicability still needs to be proved for Mg after severe plastic deformation. According to G-L model, the strain amplitude dependent component Q_h^{-1} is expressed by the equation [17]

$$\delta_h = \pi Q_h^{-1} = (C_1 / \varepsilon_0)\exp(-C_2 / \varepsilon_0) \quad (4)$$

where C_1 and C_2 are constants which are functions of dislocation density and distance between pinning points. G-L plots of pure Mg are shown in Fig.12(b). There is a good agreement between the theory and result at relatively low value of strain amplitude [18], while a deviation from the straight line occurs beyond the strain amplitude of about 5×10^{-4}, denoted as ε_{cr2}. So the IF behavior of Mg below ε_{cr2} can be explained by G-L model. The IF at higher strain amplitude may originate from another type of IF associated with plastic

deformation. And it was interpreted successfully by the IF model postulated by Peguin and his co-workers for aluminum [5]. Similar results have been obtained in other studies [19, 20]. IF related to microplasticity is characterized by the equation [5]

$$\delta_p = \pi Q_p^{-1} = \frac{A}{\varepsilon h} \exp B(\varepsilon - \varepsilon_i) \tag{5}$$

$$A = \frac{2\rho b \nu}{\pi f} \exp(-\frac{Q}{KT})$$

$$B = \alpha \frac{VG}{KT}$$

In the equations, h is a constant with the value 0.5–1, ε_i is the strain amplitude where plastic deformation starts, i.e., ε_i equals ε_{cr2}, b is the Burgers vector, ρ is the dislocation density, ν is the frequency of oscillations of the dislocations, f is the frequency of changes of loading, Q is the activation energy, α is the orientation factor (~0.5), V is the activation volume of dislocation motion, G is the shear modulus of elasticity.

From equation (5)

$$\ln \pi Q_p^{-1} \varepsilon = B\varepsilon + C \tag{6}$$

$$C = \ln A / h - B\varepsilon_i$$

If $\ln \pi Q_p^{-1} \varepsilon$ vs ε is plotted to be a straight line, the slope B of which gives the activation volume of dislocation motion. It can be seen from Fig. 13 that every curve is composed of two well-defined straight lines, so the experimental data can be explained successfully by Peguin′ s model. The critical strain corresponding to the passage of one line to the other is defined as ε_{cr3}. Hence two values of activation volume of dislocation motion are obtained, which are given in table 1.

Therefore, the dependence of IF on strain amplitude can be characterised by the equation

$$Q_{tot}^{-1}(\varepsilon) = Q_0^{-1} + Q_h^{-1}(\varepsilon) + Q_p^{-1}(\varepsilon) \tag{7}$$

As shown in Fig. 14, the strain amplitude dependent IF Q_h^{-1} and IF Q_p^{-1} related to microplasticity can be obtained by the subtraction of the background Q_0^{-1} [18]. The loading-unloading curves almost coincide with each other or show very small hysteresis loops when the strain is smaller than 1×10^{-4} (Fig. 4a), the materials almost deform in an elastic manner. At this time the dislocations reversibly motion between the weak pinning points, as shown in Fig. 15a, which only contributes to the IF background Q_0^{-1}. Above ε_{cr1} (the first critical strain amplitude) the hysteresis loops grow up gradually. This critical strain point is thought to be associated with the breakaway of dislocations from weak pinning point defects (Fig. 15b), the unpinning is a thermally activated process. In this case, the dislocations slide between the strong pinning points (Fig. 15c), and sweep large area, which results in a marked increase of anelastic strain (Fig. 9) and rapid decrease in secant elastic modulus (Fig. 10) above ε_{cr1}. The area swept by dislocations and the hysteresis loop areas determine the IF of materials. So the IF values of pure Mg increase suddenly due to the unpinning of dislocations from weak point defects above ε_{cr1} (Fig. 11). In this region only amplitude dependent component Q_h^{-1} exists after the subtraction of background Q_0^{-1} (Fig. 14),

The dislocation structure does not change after unloading until the strain amplitude reaches ε_{cr2} (the second critical strain amplitude). Above ε_{cr2} pronounced plastic deformation occurs in materials, which is associated with irreversible movement of the dislocations, accompanied by the freeing of dislocations from strong point (Fig. 15e) and generation of dislocations (Fig. 15f). In this case, some dislocation lines start to contribute to the Q_p^{-1}, while other dislocation loops still dissipate energy by reversible hysteretic mechanism of Q_h^{-1} type. Thus the Q_h^{-1} and Q_p^{-1} amplitude dependent components coexist,

and Q_h^{-1} exhibits a peak value at ε_{cr2}, the value of which is about 5×10^{-4} (Fig. 14). After the subtraction of Q_h^{-1} component, the Q_p^{-1} component exists only. In this case, the process of thermal activation is of lesser importance and the activation volume of dislocation motion increases several tens of times [4]. As shown in table 1, the values of activation volume obtained in the present study are in the same order of 10^{-27} m^3 as that of pure Mg [21, 22] and Mg-Li alloy [23] calculated by Trojanová. The intersected points at the strain of about 1×10^{-3} in Fig. 13 are corresponding to ε_{cr3} (the third critical strain amplitude). Therefore, the plastic deformation range below ε_{cr3} is related to the first microplastic defromation region of pure Mg under cyclic loading in Fig. 8(a), which is characterized by the softening of materials, in accordance with the lack of strain hardening (Fig. 8a), and as a result of the slight decrease of the friction stress in Fig. 7.

It was early reported that plastic deformation in microplastic regions in polycrystalline Mg alloys can be accommodated entirely by basal slip independent of the initial texture [24-26], since the non-basal slip systems are very difficult to be activated at room temperature, especially at the strain below the macroplastic yield point [27, 28]. The activity of the dislocation sources is accompanied by the displacement of dislocations to large distances only on basal plane in individual grain. In this case, unstable dislocation loops interact together and with a dislocation forest [29], which leads to the decrease of mobility of dislocations, and so the marked decrease of activation volume above ε_{cr3}, as shown in Fig. 13. Therefore, the deformation enters into another region corresponding to the second microplastic region in Fig. 8(b) above the plastic strain of 2×10^{-4}, which corresponds to the total strain of about 8×10^{-4} calculated by the cyclic loading curves in Fig 5. It is a little smaller than 1×10^{-3} calculated

by the IF measurements in Fig. 13. This is because IF data are measured as a function of the maximum strain amplitude, which is larger than average strain. The hardening phenomenon can also be observed in Fig. 7. The friction stress gradually increases owing to the tangle of dislocations, which can stongly block the dislocation motion.

The hardening exponents of pure Mg significantly decrease above the plastic strain of about 1×10^{-3} (Fig. 8b), i.e., the strain of about $2.5 - 2.8 \times 10^{-3}$, suggesting that the activation of other slip systems in addition to basal slip occurs above this critical strain point, which corresponds to the transition from the microstrain to the macrostrain region. The apparent elastic portion of stress-strain curve below macroscopic yield point is not a truly elastic part; rather, it is actually a rapidly work-hardened region caused by the limited slip of basal dislocations determined by the low symmetry inherent to the hexagonal structure of magnesium [30, 31].

3.5. The texture effect on internal friction (IF) and microplasticity

As shown in Figs. 3, 4 and 5, the as-extruded pure Mg exhibits the highest tensile stress in the microstrain region investigated. In general, according to Hall-Petch relationship, the macroyield strength of a polycrystalline material increases with the decrease of grain size, so does the microyielding, which takes place at much higher stresses in the finer grained samples [30, 32-34]. In the present case, though the mean grain sizes of pure Mg are substantially reduced with increasing ECAP passes, the grain size dependent strength relationship mentioned above is not established. On the contrary, for the EX-ECAPed pure Mg, the tensile strengths are reduced with the decrease of grain sizes. In fact, Texture can result in strong anisotropy and asymmetry, particularly in the case of the plastic behavior of hexagonal close

packed (hcp) magnesium and its alloys. Thus texture has a great effect on microplasticity as well as macroplasticity. It was reported that the initial microyielding behavior in Mg alloys is only involved with a limited number of grains oriented favorably for basal slip, while other grains remain largely elastic [24, 26, 32, 35, 36], suggesting that the microyield stress decreases with increasing average Schmid factor of the basal slip mode [24, 32]. As shown in Fig. 2, the as-extruded alloy exhibits a typical fiber texture, with $(0002)<10\bar{1}0>$ almost parallel to the extrusion axis. With increasing ECAP passes, most of the basal planes rotate gradually from 0º to 40º towards ED. Thus if the specimens are loaded in ED, the ECAPed samples will have much higher Schmid factor for basal slip. It means the dislocation networks are easy to slide on basal plane at same external stress. Therefore, the ECAP-4P sample shows the most pronounced plastic and anelastic behavior but lowest friction stress of dislocation motion and secant elastic modulus. Moreover, the critial strain amplitudes for unpinning from weak and strong points (ε_{cr1} and ε_{cr2}) slightly decrease with an increase of ECAP passes, as shown in table 1. It was noted that the grain refinement below 10μm may lead to the decrease of strain amplitude dependent internal friction due to the rapid increase of area of grain boundaries which are strong pinning points of dislocations [37]. However, the ECAP-4P pure Mg that has the smallest grain size shows the largest IF value and activated volume, suggesting that texture plays a dominant role in the present case.

4. Conclusions

Equal channel angular pressing (ECAP) was performed on the as-extruded commercial pure magnesium. The microplastic deformation and internal friction mechanisms and their relationship were studied in detail by the cyclic loading and internal friction experiments.

(1) The grain size of pure Mg is significantly refined after ECAP processing, and a new stronger texture component with basal planes with basal planes having a tilting angle of about 35º to the extrusion direction appears.

(2) The internal friction of Mg at high strain amplitude is closely associated with microplastic deformation and can be interpreted by dislocation mechanism. The Granato and Lücke model only satisfies in anelastic region, while the internal friction in microplastic deformation region should be explained in terms of the Peguin′ s internal friction model related to microplasticity.

(3) The microplastic deformation process can be divided into two regions, which is proved by both the cyclic loading and IF measurements. Pronounced plastic deformation related to displacement of dislocations to large distance on basal plane have already taken place below the strain of 5×10^{-4}. The materials are softened. When reaching the strain of about 1×10^{-3}, the microplasctic deformation enters into region II. Annihilation and tangle of dislocations lead to the decrease of the activation volume of dislocation motion and the increase of hardening exponents and friction stress. The transition from the microstrain to the macrostrain region occurs at the strain of about $(2.5 - 2.8) \times 10^{-3}$.

(4) Texture has a great effect on the microplasticity of pure Mg. With increasing the number of ECAP passes, the Schmid factor for basal slip increases. Larger Schmid factor will contribute to larger internal friction but smaller tensile stress in microstrain region. And the ECAP-4P sample shows the most pronounced plastic and anelastic behavior but lowest friction stress and secant elastic modulus.

Acknowledgements

This work was supported by the National Nature Science Foundation of China (No. 50571031, No.50801017 and No.51071057) and PPP project (No. 2007-3086, Project based Personnel Exchange Program with China Scholarship Council (CSC) and German Academic Exchange Service (DAAD)).

References

[1] Q. Li, Q. Yu, J. Zhang, Y. Jiang, Scripta Mater. 62 (2010) 778-781.

[2] S. H. Park, S. Hong, W. Bang, C. S. Lee, Mater. Sci. Eng. A 527 (2010) 417-423.

[3] F. Zhang, P. Sun, X. Li, G. Zhang, Mater. Lett. 49 (2001) 69-74.

[4] A. Puškár, Internal Friction of Materials, Cambridge International Science Publishing, Cambrigde, 2001.

[5] P. Peguin, J. Perez, P. Gobin, Trans. Metall. Soc. AIME 239 (1967) 438-450.

[6] C. F. Burdett, J. Phys. D: Appl. Phys. 4 (1971) 2017-2021.

[7] R. B. Figueiredo, T. G. Langdon, Mater. Sci. Eng. A 501 (2009) 105-114.

[8] W. J. Kim, S. I. Hong, Y. S. Kim, S. H. Min, H. T. Jeong, J. D. Lee, Acta Mater. 51 (2003) 3293-3307.

[9] V. N. Chuvil'deev, T. G. Nieh, M. Y. Gryaznov, V. I. Kopylov, A. N. Sysoev, J. Alloys Compd 378 (2004) 253-257.

[10] G. D. Fan, M. Y. Zheng, X. S. Hu, H. Chang, K. Wu, Int. J. Mod. Phys. B 23 (2009) 1829-1833.

[11] S. B. Yi, C. H. Davies, H.-G. Brokmeier, R. E. Bolmaro, K. U. Kainer, J. Homeyer, Acta Mater. 54 (2006) 549-562.

[12] G. V. Seregin, L. L. Efimenko, M. V. Leonov, Met. Sci. Heat Treat. 37 (1995) 70-73.

[13] A. F. Armas, S. Hereñú, R. Bolmaro, I. Alvarez-Armas, Rev. Mater. 9 (2004) 280-287.

[14] S. Chen, X. Dong, R. Ma, L. Zhang, H. Wang, Z. Fan, Mater. Sci. Eng. A 551 (2012) 87-94.

[15] Z. Zhang, L. Peng, X. Zeng, L. Du, L. Ma, W. Ding, Mater. Sci. Forum 546-549 (2007) 257-260.

[16] Z. Zhang, X. Zeng, W. Ding, Mater. Sci. Eng. A 392 (2005) 150-155.

[17] A. Granato, K. Lücke, J. Appl. Phys. 27 (1956) 583-593.

[18] G. D. Fan, M. Y. Zheng, X. S. Hu, C. Xu, K. Wu, I. S. Golovin, Mater. Sci. Eng. A 556 (2012) 588-594.

[19] C. F. Burdett, Philos. Mag. 24 (1971) 1459-1464.

[20] R. González-Martínez, J. Göken, D. Letzig, J. Timmerberg, K. Steinhoff, K. U. Kainer, Acta Metall. Sin. 20 (2007) 235-240.

[21] Z. Trojanová, Z. Drozd, P. Lukac, K. Mathis, H. Ferkel, W. Riehemann, Scripta Mater. 42 (2000) 1095-1100.

[22] Z. Trojanová, B. Weidenfeller, P. Lukác, W. Riehemann, M. Stank, Nanomaterials by Severe Plastic Deformation 7 (2005) 413-419.

[23] Z. Trojanova, P. Lukac, W. Riehemann, Defect and Diffusion Forum 203-205 (2002) 249-252.

[24] Y. B. Chun, C. H. J. Davies, Mater. Sci. Eng. A 528 (2011) 3489-3495.

[25] O. Muránsky, D. G. Carr, M. R. Barnett, E. C. Oliver, P. Sittner, Mater. Sci. Eng. A 496 (2008) 14-24.

[26] S. R. Agnew, D. W. Brown, C. N. Tom, Acta Mater. 54 (2006) 4841-4852.

[27] T. Obara, H. Yoshinga, S. Morozumi, Acta Metall. 21 (1973) 845-853.

[28] W. F. Sheerly, R. R. Nash, Trans. Metall. Soc. AIME 218 (1960) 416-423.

[29] M. C. Jon, W. P. Mason, D. N. Beshers, J. Appl. Phys. 47 (1976) 2337-2349.

[30] J. Koike, Metall. Mater. Trans. A 36 (2005) 1689-1696.

[31] J. Koike, T. Kobayashi, T. Mukai, H. Watanabe, M. Suzuki, K. Maruyama, K. Higashi, Acta Mater. 51 (2003) 2055-2065.

[32] B. Raeisinia, S. R. Agnew, Scripta Mater. 63 (2010) 731-736.

[33] D. A. Thomas, B. L. Averbach, Acta Metall. 7 (1959) 69-75.

[34] N. Brown, K. F. Lukens, Acta Metall. 9 (1961) 106-111.

[35] S. R. Agnew, C. N. Tom, D. W. Brown, T. M. Holden, S. C. Vogel, Scripta Mater. 48 (2003) 1003-1008.

[36] B. Clausen, C. N. Tom, D. W. Brown, S. R. Agnew, Acta Mater. 56 (2008) 2456-2468.

[37] K. Sugimoto, K. Niiya, T. Okamoto, K. Kishitake, Trans. JIM 18 (1977) 277-288.

List of figure captions

Fig. 1. Optical micrographs of the pure Mg after (a) extrusion and subsequent ECAP processing at 250^{o}C for (b) 1 pass, (c) 2 passes and (d) 4 passes.

Fig. 2. (0002) and $(10\bar{1}0)$ complete pole figures of the extruded and ECAP processed pure Mg from 1 to 4 passes.

Fig. 3. The tensile stress-strain curves of the extruded and ECAPed pure Mg in microstrain range.

Fig. 4. Tensile loading–unloading loops measured by DMA for pure Mg after (a) extrusion and subsequent ECAP processing for (b) 1 pass, (c) 4 passes.

Fig. 5. Tensile loading–unloading loops measured by tensile machine for pure Mg after (a) extrusion and subsequent ECAP processing for (b) 1 pass, (c) 4 passes.

Fig. 6. Schematic flow curve of cyclic loading hysteresis loops. E is the elastic modulus of Mg (42MPa), E_s is the secant modulus. ε_p and ε_e are the plastic strain and elastic strain;

ε_a is the anelastic strain during unloading. σ_p is the peak stress at the start of the unloading; σ_f and σ_b are the friction stress and back stress, respectively; σ_y is the yield stress upon unloading.

Fig. 7. The development of friction stress as a function total strain for pure Mg.

Fig. 8. The relationship between the stress amplitude and plastic strain of pure Mg in (a) smaller strain and (b) larger strain region.

Fig. 9. The anelastic strain as a function of the total strain of pure Mg in (a) smaller strain and (b) larger strain region.

Fig. 10. The development of normalized secant elastic modulus as a function true strain.

Fig. 11. The strain amplitude dependence of internal friction of pure Mg.

Fig. 12. G-L plots of pure Mg.

Fig. 13. Plastic strain internal friction $\ln(\pi\varepsilon Q_p^{-1})$ plotted as function of strain.

Fig. 14. Schematic diagram of amplitude dependent internal friction Q_h^{-1} and plastic internal friction Q_p^{-1} after the subtraction of amplitude independent internal friction Q_0^{-1} [18].

Fig. 15. Dislocation model of microplasticity according to Granato-Lücke theory [17].

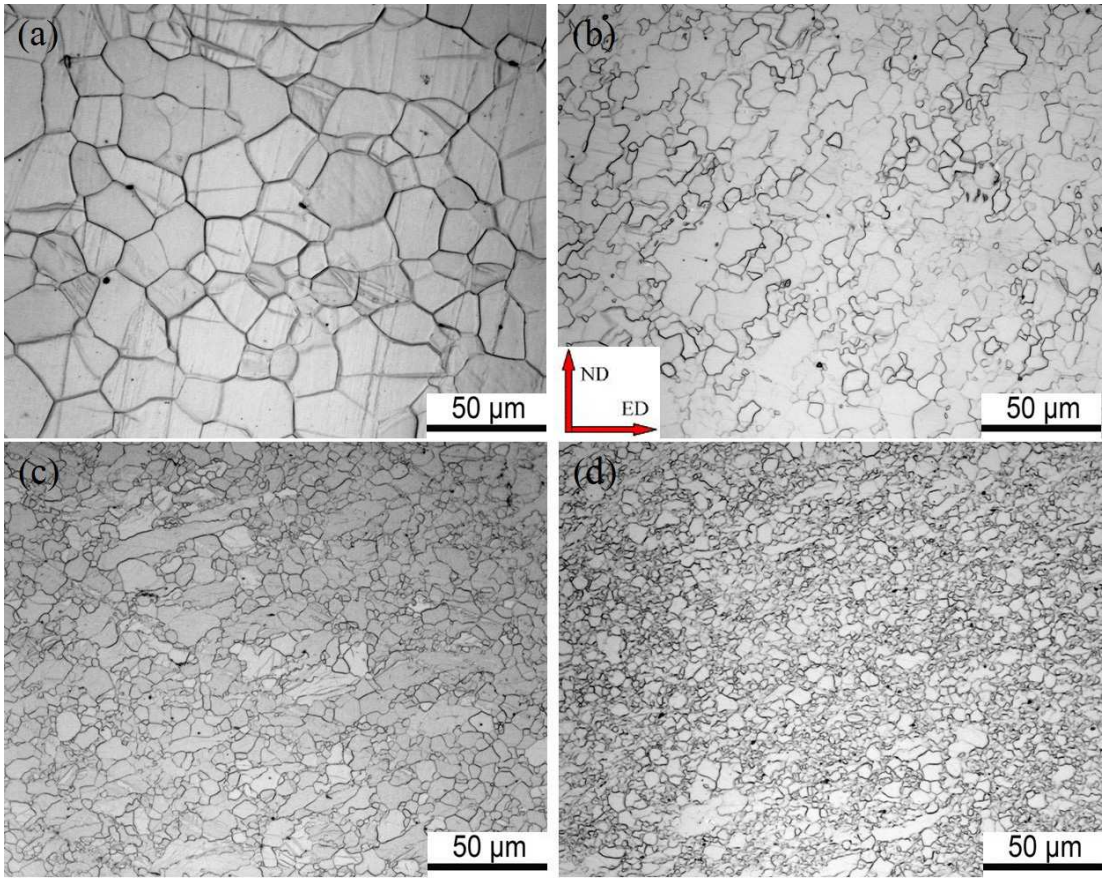

Fig. 1. Optical micrographs of the pure Mg after (a) extrusion and subsequent ECAP processing at 250°C for (b) 1 pass, (c) 2 passes and (d) 4 passes.

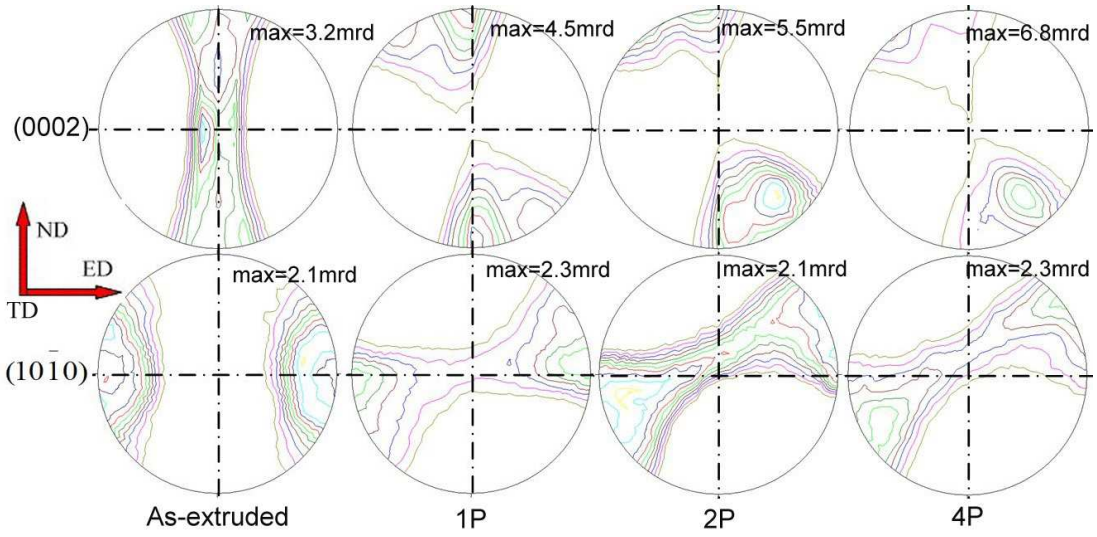

Fig. 2. (0002) and $(10\bar{1}0)$ complete pole figures of the extruded and ECAP processed pure Mg from 1 to 4 passes.

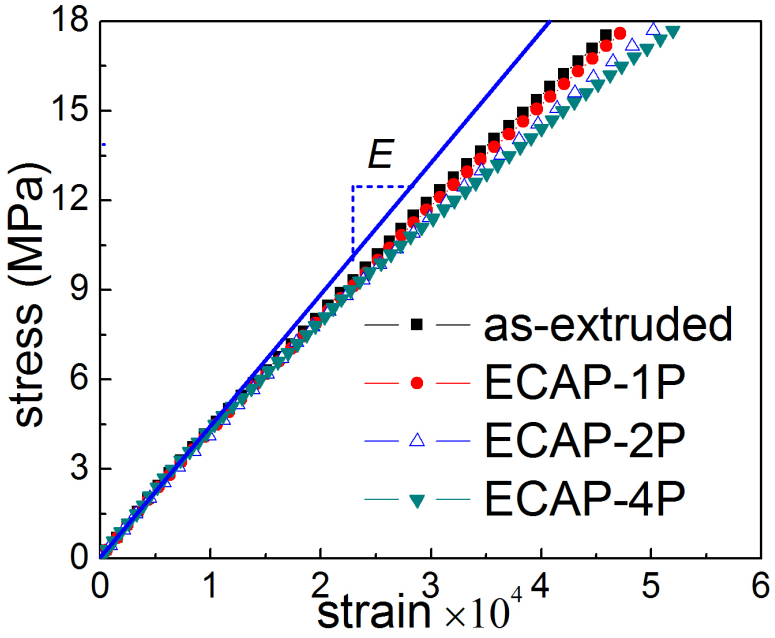

Fig. 3. The tensile stress-strain curves of the extruded and ECAPed pure Mg in microstrain range.

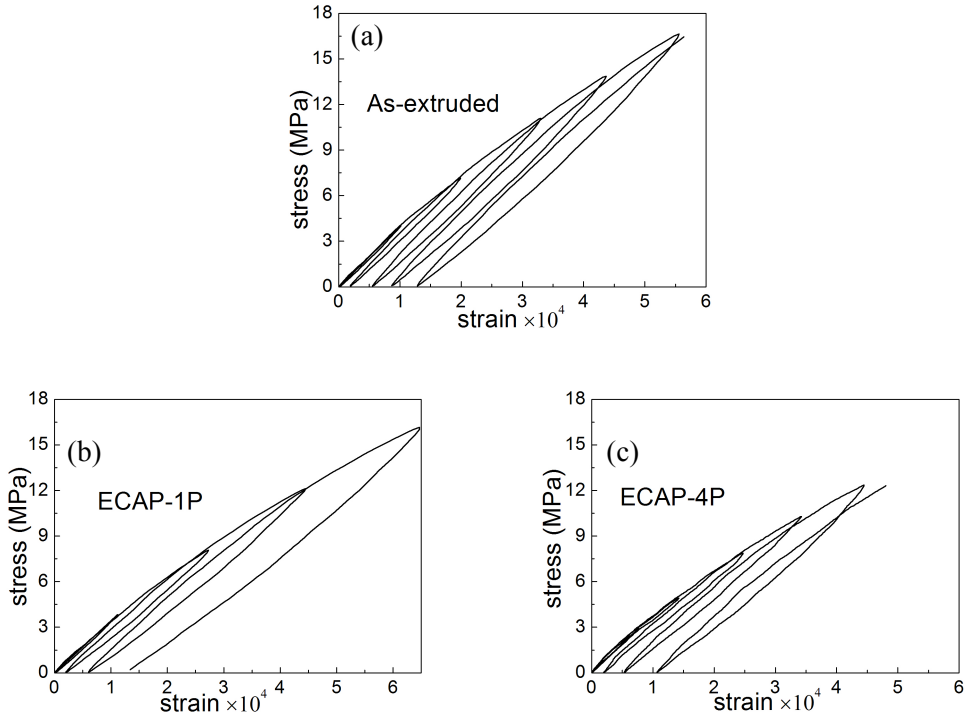

Fig. 4. Tensile loading–unloading loops measured by DMA for pure Mg after (a) extrusion and subsequent ECAP processing for (b) 1 pass, (c) 4 passes.

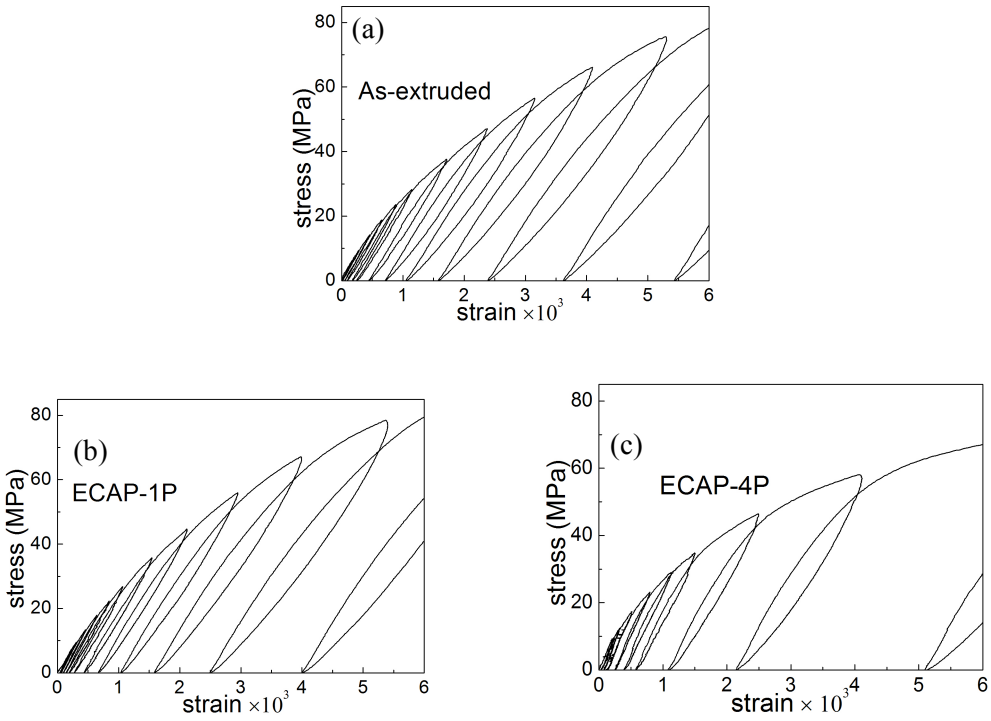

Fig. 5. Tensile loading–unloading loops measured by tensile machine for pure Mg after (a) extrusion and subsequent ECAP processing for (b) 1 pass, (c) 4 passes.

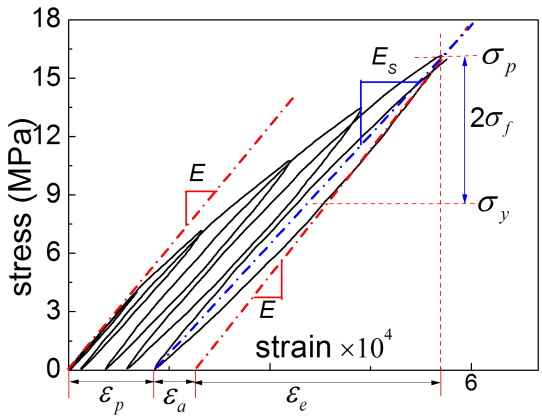

Fig. 6. Schematic flow curve of cyclic loading hysteresis loops. E is the elastic modulus of Mg (42MPa), E_s is the secant modulus. ε_p and ε_e are the plastic strain and elastic strain; ε_a is the anelastic strain during unloading. σ_p is the peak stress at the start of the unloading; σ_f and σ_b are the friction stress and back stress, respectively; σ_y is the yield stress upon unloading.

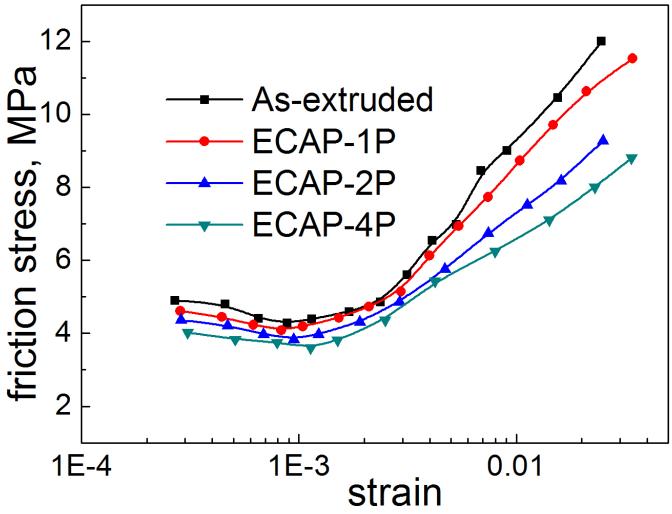

Fig. 7. The development of friction stress as a function total strain for pure Mg.

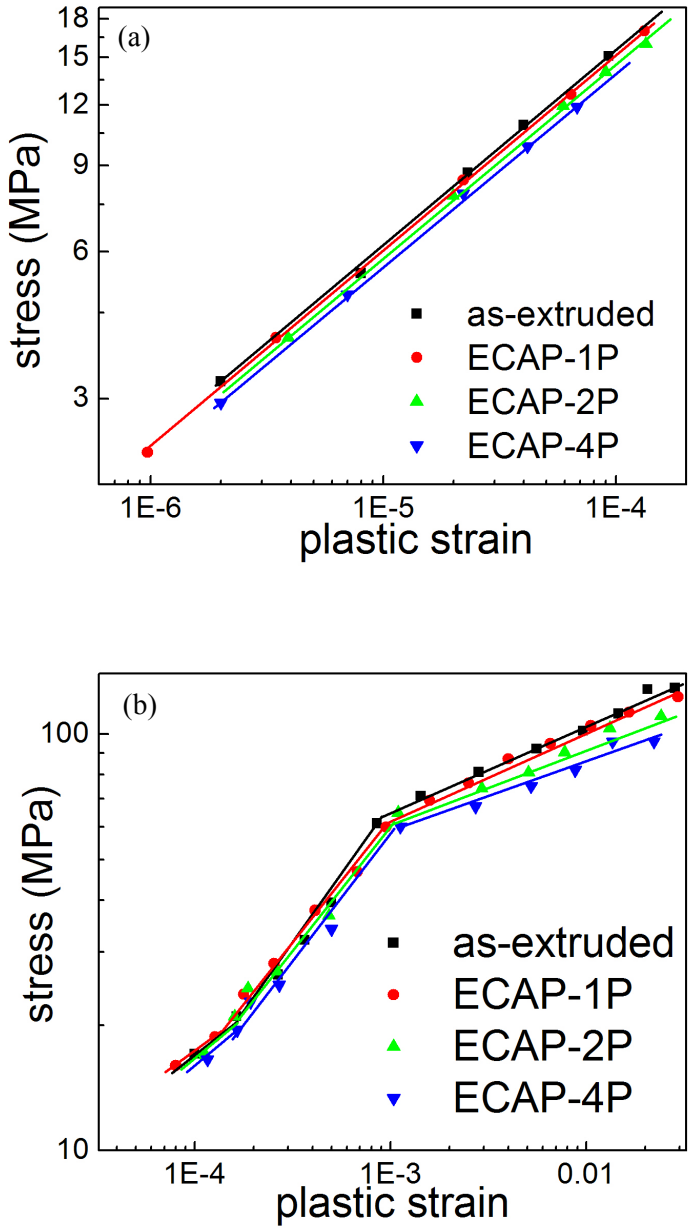

Fig. 8. The relationship between the stress amplitude and plastic strain of pure Mg in (a) smaller strain and (b) larger strain region.

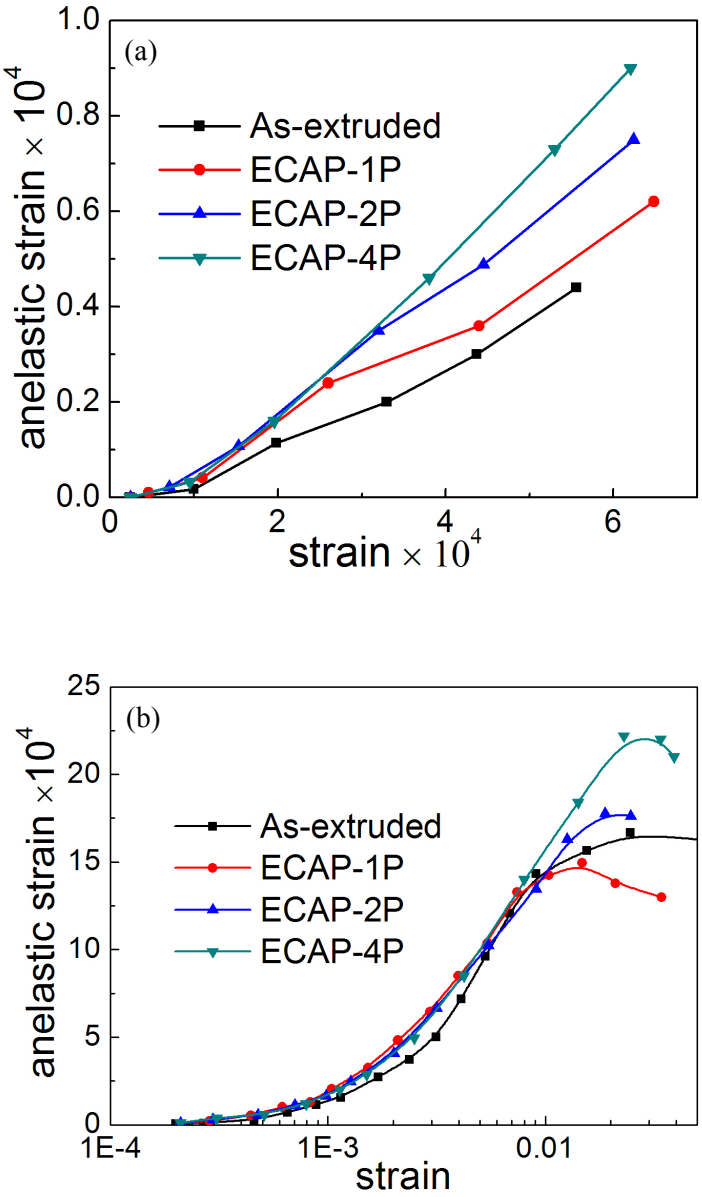

Fig. 9. The anelastic strain as a function of the total strain of pure Mg in (a) smaller strain and (b) larger strain region.

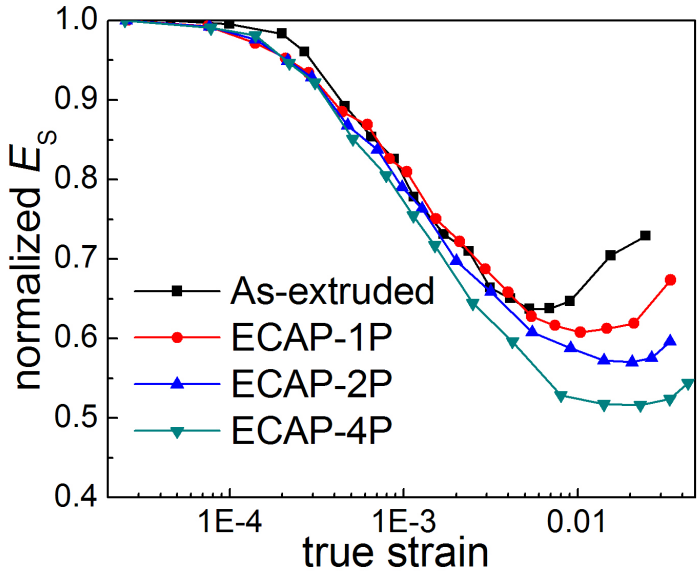

Fig. 10. The development of normalized secant elastic modulus as a function true strain.

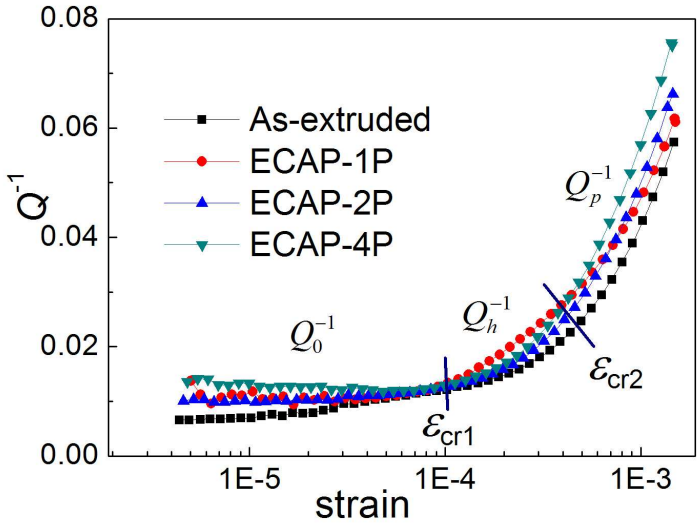

Fig. 11. The strain amplitude dependence of internal friction of pure Mg.

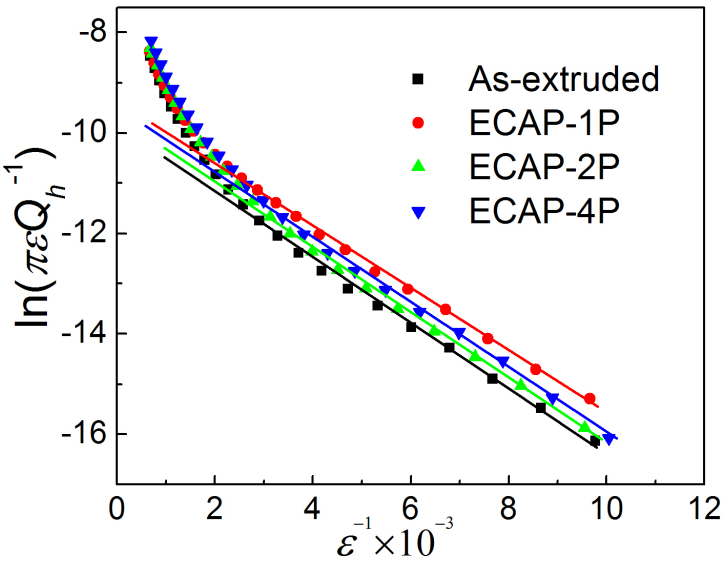

Fig. 12. G-L plots of pure Mg.

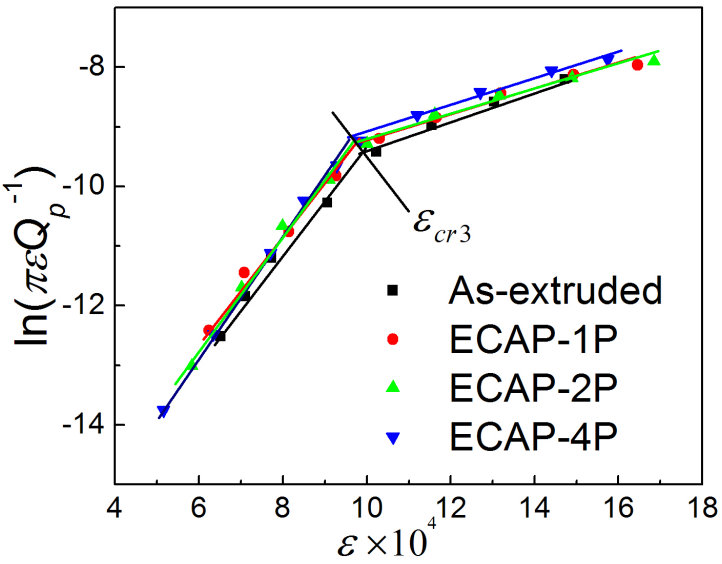

Fig. 13. Plastic strain internal friction $\ln(\pi\varepsilon Q_p^{-1})$ plotted as function of strain.

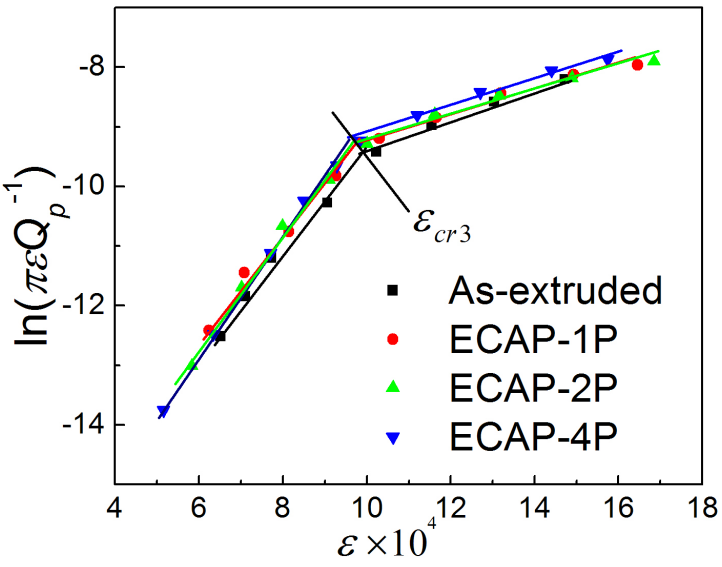

Fig. 13. Plastic strain internal friction $\ln(\pi\varepsilon Q_p^{-1})$ plotted as function of strain.

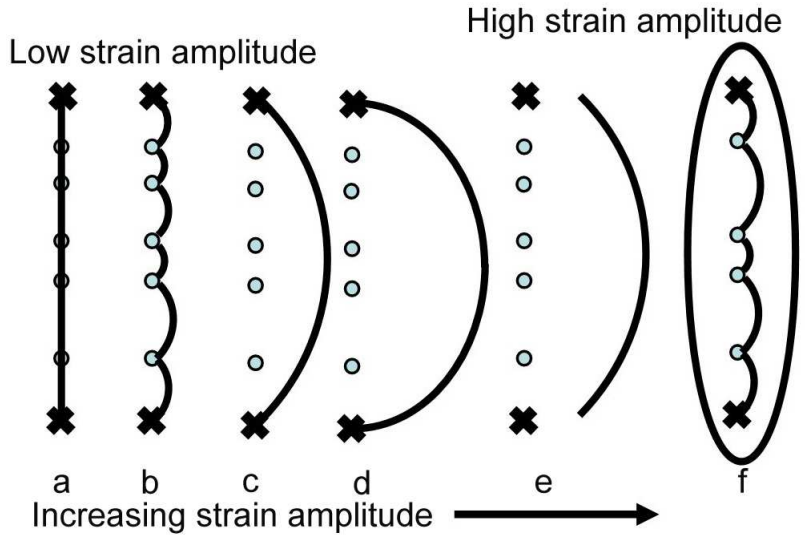

Fig. 15. Dislocation model of microplasticity according to Granato-Lücke theory [17].

Table 1. Experimentally determined exponents and factors of microplastic response

Materials	Hardening exponents			Critical strains			Activation volumes			
	n_1	n_2	n_3	ε_{cr1} $\times 10^4$	ε_{cr2} $\times 10^4$	ε_{cr3} $\times 10^4$	$V_1 \times 10^{-27}$ (m^3)	V_1 / b^3	$V_2 \times 10^{-27}$ (m^3)	V_2 / b^3
As-extruded	0.40	0.60	0.20	0.93	5.86	9.92	1.62	50	0.62	19
ECAP-1P	0.40	0.57	0.20	0.83	5.57	9.81	1.68	51	0.61	19
ECAP-2P	0.39	0.56	0.18	0.87	5.36	9.79	1.84	56	0.61	19
ECAP-4P	0.39	0.57	0.16	0.82	5.15	9.54	2.03	62	0.61	19